Journal of Modern Optics
Vol. 00, No. 00, DD Month 200x, 1–14

High-order harmonic generation in vibrating molecules

C. C. CHIRILĂ and M. LEIN
Max Planck Institute for Nuclear Physics,
Saupfercheckweg 1, 69117 Heidelberg, Germany
(Received 00 Month 200x; In final form 00 Month 200x)

The generation of high-order harmonics in small diatomic molecules is theoretically investigated with inclusion of the vibrational degree of freedom. The results obtained from the solution of the time-dependent Schrödinger equation for a model H_2 molecule are interpreted by analyzing the influence of the vibrational motion in the framework of the strong-field approximation. Ionization launches a vibrational wave packet whose motion is correlated with the motion of the continuum electron wave packet. The harmonics are sensitive to a correlation function quantifying the overlap between the vibrational wave packet at the time of recombination and a vibrational target wave packet, i.e. the wave packet for which deexcitation into the ground state is most likely. We show that more intense harmonics are generated in heavier isotopes due to the slower nuclear motion.

Keywords: Harmonic generation; Strong-field approximation; Vibrating molecules

1 Introduction

In a series of recent experiments, it has been demonstrated that sub-fs-duration electron wave packets that are created in the interaction of molecules with strong laser fields can be utilized to probe the structure and dynamics of molecules [1–4]. The underlying physical mechanism is a three-step process [5, 6] consisting of strong-field ionization, acceleration of the free electron and recollision with the parent ion. Since recollisions can resolve the dynamics of the molecular ion on a sub-fs time scale, this field of research is becoming a branch of attosecond physics. The earliest proposal to use recollisions for imaging of molecular structure considered the diffraction of the returning electron as it scatters elastically from the core [7]. The first experiments [1–3] focussed instead on inelastic recollisions leading to dissociation, with information about the molecular geometry at the time of recollision being encoded in the fragment energies.

More recently, high-order harmonic generation (HHG), i.e. recombination of the returning electron resulting in the emission of a photon, has emerged as another promising possibility to achieve molecular imaging. The sensitivity of harmonics to the molecular orientation was first seen in experiments with

adiabatically aligned molecules [8]. The prediction of interferences in HHG due to molecular structure [9–12] prompted more intensive research in this direction [13, 14]. In the experiment of Ref. [4], the valence orbital of the N_2 molecule was reconstructed from HHG spectra by applying a tomographic technique.

Although most of the theoretical research on molecules in strong fields employs fixed nuclei, the inclusion of the nuclear motion has received growing attention in the last years. So far, however, the main focus has been on the question which vibrational levels are populated in the molecular ion [15–19].

In this article, we review the influence of molecular vibrations on HHG [20]. It is shown that not only the structure but also the laser-induced dynamics of molecules is encoded in HHG spectra. In Section 2, we first review results of numerical Schrödinger-equation simulations. In Section 3, we extend the analytical theory of Ref. [20] to give a more precise picture of the mechanism of harmonic generation in the presence of nuclear motion. In particular, we introduce the notion of a vibrational 'target' wave packet. HHG is only possible if the vibrational wave packet at the time of recollision has a non-negligible overlap with the target wave packet. The latter had been taken identical to the initial vibrational wave packet in the simpler theory of Ref. [20].

2 Numerical results

The coupled electronic and nuclear wave packet dynamics should be described in a non-Born-Oppenheimer (non-BO) treatment, since the BO approximation breaks down for the highly excited states that are populated in the course of intense-laser molecule interaction. While for the H_2^+ molecular ion and simplified models thereof, a number non-BO calculations have been carried out [21], little work has been done for neutral molecules [22, 23]. In this section, we investigate a non-BO model of H_2 with two-dimensional electron dynamics and one-dimensional nuclear dynamics. The direction of the molecular axis, given by the angle θ between molecular axis and electric field $\mathbf{E}(t)$ of the laser, is fixed but arbitrary, so that we can study the influence of the molecular orientation. The amplitude of the electric field is $\mathcal{E}_0$. We employ a single-active-electron approach where only one of the two electrons can be excited by the laser. Using velocity gauge, the single-active-electron Hamiltonian for the interaction with a linearly polarized laser field along the x-axis reads (atomic units are used throughout)

$$H_{\rm eff} = -\frac{\partial_R^2}{M} - \frac{1}{2}\nabla_{\boldsymbol{r}}^2 - i\,A(t)\frac{\partial}{\partial x} + V_{\rm eff}(R,\boldsymbol{r}), \tag{1}$$

where $A(t) = -\int_{-\infty}^{t} E(t')\,dt'$, M is the mass of one nucleus, $\boldsymbol{r}$ is the electron coordinate and R is the internuclear distance. (The deviation of the reduced electron mass from unity is neglected.) The interaction between the active electron and the core could in principle be calculated in the spirit of a BO approximation for the inner electron only. Here, we prefer to simply assume a reasonable form of interaction, chosen such that is satisfies a number of important conditions. We use

$$V_{\rm eff}(R,\boldsymbol{r}) = V_{\rm BO}^{+}(R) - \sum_{j=1,2} \frac{Z(R,|\boldsymbol{r}-\boldsymbol{R}_j|)}{\sqrt{|\boldsymbol{r}-\boldsymbol{R}_j|^2+0.5}}, \tag{2}$$

where $\boldsymbol{R}_j$ are the positions of the nuclei. For $|\boldsymbol{r}| \to \infty$ this function approaches $V_{\rm BO}^{+}(R)$, the lowest BO potential of H_2^+. This means that the removal of one electron creates H_2^+ in its electronic ground state. The second term is a soft-core interaction that models the attractive potential due to the core. We have introduced an effective nuclear charge $Z(R,u) = \{1+\exp[-u^2/\sigma^2(R)]\}/2$, which mimics the average screening of the nuclei by the inner electron: $Z(R,u) \to 1$ for $u \to 0$, and $Z(R,u) \to 1/2$ for $u \to \infty$. We adjust the R-dependence of the screening parameter $\sigma(R)$ such that the resulting lowest BO potential of the neutral model molecule matches the real H_2 BO potential (data taken from the calculation of Ref. [24]). Hence, our model is capable of describing the nuclear motion correctly, both in the neutral and in the ionized molecule.

The wave function $\Phi(R,\boldsymbol{r},t)$ is represented in Cartesian coordinates, and the time-dependent Schrödinger equation $i\partial\Phi/\partial t = H_{\rm eff}\Phi$ is solved numerically using the split-operator method [25], starting from the ground state of the system. Absorbing boundaries are employed for all coordinates. The spectrum of emitted radiation is calculated by Fourier transforming the time-dependent dipole acceleration [26]. A grid size of $L_x \times L_y = 180 \times 45$ a.u. is used for the electron, and the internuclear distance is allowed to be in the range $R = [0.6\,\text{a.u.}, 3.7\,\text{a.u.}]$.

Figure 1 shows the calculated harmonic spectra for various orientations of H_2 in a 780 nm pulse with intensity $4\times10^{14}\,\text{W/cm}^2$. Trapezoidally shaped 6-cycle laser pulses have been used. The cut-off at the photon energy $3.17U_{\rm p}+I_{\rm p}$ [5,6] is clearly visible in all spectra. Here, $U_{\rm p} = \mathcal{E}_0^2/(4\omega^2)$ is the ponderomotive potential and $I_{\rm p}$ is the vertical ionization potential.

For sufficiently small θ, the spectrum exhibits a minimum due to two-centre interference as described for clamped nuclei in Refs. [9–11]. Obviously, the minimum persists when the vibrational motion is taken into account. However, it is shifted towards smaller harmonic frequencies as compared to Ref. [9]. This indicates that the internuclear distance during the HHG process is slightly

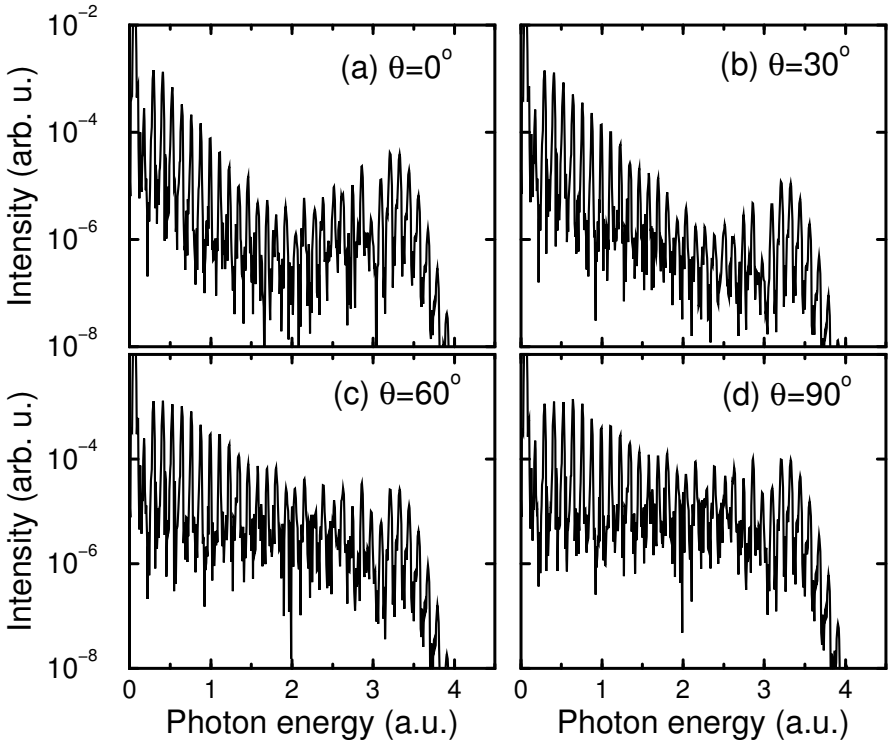

Figure 1. Calculated harmonic spectra for various orientations of H_2 in a 780 nm pulse with 4×10^{14} W/cm^2 intensity.

larger than the equilibrium distance 1.4 a.u. On one hand, this is consistent with the picture of a vibrational wave packet leading to an expansion of the molecule between ionization and recombination. On the other hand, the dependence of the ionization probability on the internuclear distance may also give increased weight to larger distances.

To investigate the influence of vibrations in more detail, we proceed with a comparison of the isotopes H_2 and D_2 since these two species have identical electronic structure but differ in their nuclear dynamics.

In figure 2, we compare the harmonics from H_2 and D_2 aligned perpendicular to the field. This orientation is chosen because it does not give rise to a two-centre interference pattern. We consider two different laser wavelengths, 780 nm and 1200 nm. In both cases we clearly observe that the heavier isotope generates more intense harmonics. Plotted is for each odd harmonic the ratio between the yields integrated over one harmonic peak. The ratio between the isotopes is approximately unity for the lowest harmonic orders. The ratio tends to grow with increasing harmonic order, but in addition it exhibits fast oscillations. It is noticeable that this modulation is most pronounced near the

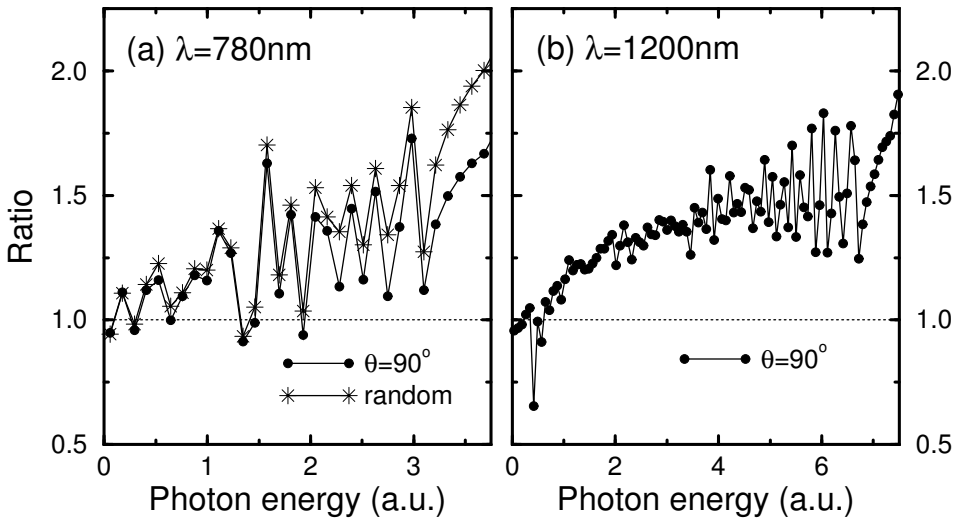

Figure 2. Ratio between harmonic intensities in the isotopes D_2 and H_2 aligned perpendicular to the laser field for odd harmonics from 780 nm laser wavelength [panel (a)] and 1200 nm laser wavelength [panel (b)]. Panel (a) includes also the ratio for randomly oriented molecules. The laser intensity is 4×10^{14} W/cm^2.

cut-off. An average ratio of about 1.5 is reached at the cut-off.

The theoretical description of a randomly oriented ensemble, which is more easily accessible by experiment, requires the calculation of the harmonic intensities and phases for all orientations, and these contributions have to be added coherently [27]. This analysis has been carried out for the 780 nm case, see figure 2(a). The resulting ratio resembles the case of perpendicular alignment. The ratio is even slightly enhanced. The similarity arises because the contributions near $\theta = 90^o$ dominate the signal in the random ensemble for two reasons: (a) the contributions are weighted by a geometrical factor $\sin\theta$ [27]; (b) two-centre interference is constructive around $\theta = 90^o$ [10]. Despite this similarity, the harmonic signal is much higher in the aligned ensemble as can be seen in figure 3. This difference stems not only from the fact that HHG is maximized at $\theta = 90^o$, but also from phase mismatch between different orientations in the randomly oriented ensemble.

3 Strong-field approximation including nuclear motion

To obtain more insight into the physics of HHG in molecules, it is desirable to have a semianalytical description. To this end, we adopt and extend the strong-field approximation (SFA) for molecules developed in Ref. [20]. We proceed similar to the Lewenstein model of HHG in atoms [28]. The length-gauge Hamiltonian for a H_2 molecule with fixed orientation, irradiated by a

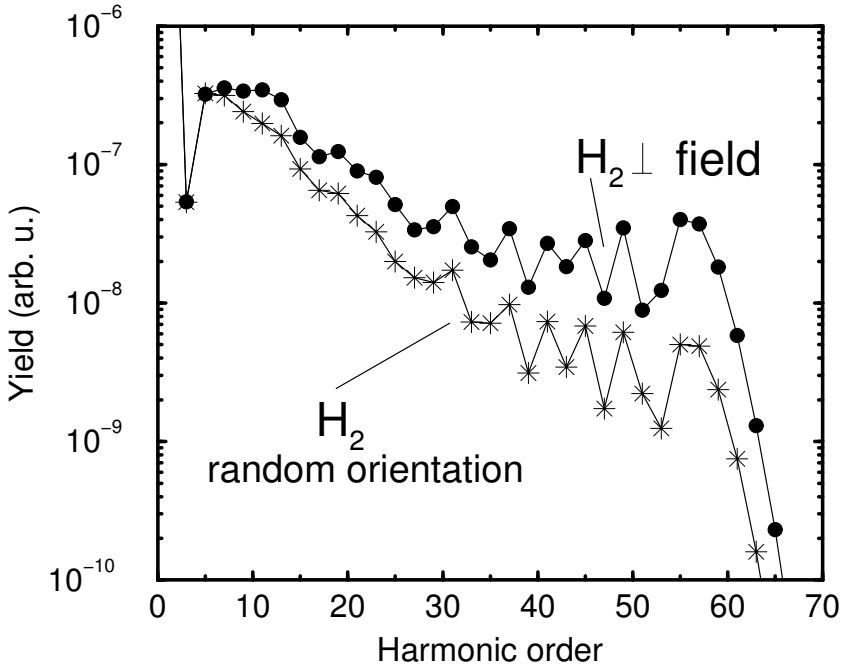

Figure 3. Comparison of harmonics generated by H_2 aligned perpendicular to the laser field and by randomly oriented H_2 molecules in a 780 nm pulse with intensity 4×10^{14} W/cm^2. (Intensity integrated over one peak for each odd harmonic.)

linearly polarized laser field along the x axis, reads

$$H = -\frac{\nabla_1^2}{2} - \frac{\nabla_2^2}{2} - \frac{\partial_R^2}{M} + V(\boldsymbol{r}_1, \boldsymbol{r}_2, R) + E(t)(x_1 + x_2), \tag{3}$$

where $\boldsymbol{r}_1$, $\boldsymbol{r}_2$ are the electron coordinates, R is the internuclear distance, and V is the sum of the Coulomb interactions between all particles. Following Ref. [28], we assume that (a) no bound states other than the BO ground state are populated, (b) the depletion of the ground state can be neglected, and (c) while in the continuum, the active electron does not interact with the core. Additionally, we assume that only a single electron can become active, i.e. if one of the electrons has been excited into the continuum, the second electron will not couple to the field and will always remain in the lowest BO state of the molecular ion.

We can then expand the full wave function as

$$\Psi(\boldsymbol{r}_1, \boldsymbol{r}_2, R, t) = e^{-iE_0 t}\Big\{\Psi_0(\boldsymbol{r}_1, \boldsymbol{r}_2, R) + \int \frac{d^3k}{(2\pi)^3}\,\phi(\boldsymbol{k}, R, t)$$

$$\times [e^{i\boldsymbol{k}\cdot\boldsymbol{r}_1}\psi_R^+(\boldsymbol{r}_2) + e^{i\boldsymbol{k}\cdot\boldsymbol{r}_2}\psi_R^+(\boldsymbol{r}_1)]\Big]\Big\}, \tag{4}$$

where $\Psi_0(\boldsymbol{r}_1, \boldsymbol{r}_2, R) = \chi_0(R)\psi_R(\boldsymbol{r}_1, \boldsymbol{r}_2)$ is the real-valued ground-state wave function of H_2/D_2 in the BO approximation, E_0 is the ground-state energy, and $\psi_R^+(\boldsymbol{r})$ is the electronic ground-state BO wave function of H_2^+. Neglecting the non-BO couplings and laser-field interaction for ψ_R^+, the time-dependent Schrödinger equation $i\partial\Psi/\partial t = H\Psi$ is transformed to

$$\dot{\phi}(\boldsymbol{k}, R, t) = -i\left[\frac{\boldsymbol{k}^2}{2} - \frac{\partial_R^2}{M} + V_{\rm BO}^+(R) - E_0\right]\phi(\boldsymbol{k}, R, t) + E(t)\frac{\partial\phi(\boldsymbol{k}, R, t)}{\partial k_x} - i\,E(t)d_{\rm ion}(\boldsymbol{k}, R)\,\chi_0(R), \tag{5}$$

where $d_{\rm ion}(\boldsymbol{k}, R) = \langle \exp(i\boldsymbol{k}\cdot\boldsymbol{r}_1)\psi^+(\boldsymbol{r}_2)|x_1|\psi_R(\boldsymbol{r}_1, \boldsymbol{r}_2)\rangle$ describes the detachment of the active electron. To find the solution, one can make the substitution $\phi(\boldsymbol{k}, R, t) = \exp\{-i\hat{H}_R t\}\tilde{\phi}(\boldsymbol{k}, R, t)$, where $\hat{H}_R$ is the Hamiltonian governing the nuclear dynamics:

$$\hat{H}_R = -\frac{\partial_R^2}{M} + V_{\rm BO}^+(R). \tag{6}$$

The equation satisfied by the new function is similar to (5), but the nuclear motion is moved into the inhomogeneous term:

$$\dot{\tilde{\phi}}(\boldsymbol{k}, R, t) = -i\left[\frac{\boldsymbol{k}^2}{2} - E_0\right]\tilde{\phi}(\boldsymbol{k}, R, t) + E(t)\frac{\partial\tilde{\phi}(\boldsymbol{k}, R, t)}{\partial k_x} - i\,E(t)e^{i\hat{H}_R t}d_{\rm ion}(\boldsymbol{k}, R)\,\chi_0(R). \tag{7}$$

This is the same as in the Lewenstein model of HHG for atoms, but now the inhomogeneous term depends on the internuclear distance. Before arriving at the final expression for the dipole moment, we write $d_{\rm ion}(\boldsymbol{k}, R)\chi_0(R) = \bar{d}(\boldsymbol{k})\eta_{\boldsymbol{k}}(R)$, where $\eta_{\boldsymbol{k}}(R)$ is a normalized wave packet. The normalization condition is fulfilled by choosing $\bar{d}(\boldsymbol{k}) = (\int |d_{\rm ion}(\boldsymbol{k}, R)\chi_0(R)|^2 dR)^{1/2}$. This 'effective' matrix element is the molecular counterpart of the matrix element appearing in the Lewenstein model for HHG in atoms, only averaged over all possible values of the internuclear distance R.

Solving for $\tilde{\phi}$ under the initial condition $\tilde{\phi}(\boldsymbol{k}, R, 0) = 0$ and transforming

back to the original function gives:

$$\phi(\boldsymbol{k},R,t) = -i\int_0^t dt'\, E(t')\bar{d}[\boldsymbol{k}-\boldsymbol{A}(t)+\boldsymbol{A}(t')]\, e^{-i\hat{H}_R(t-t')}\eta_{\boldsymbol{k}-\boldsymbol{A}(t)+\boldsymbol{A}(t')}(R) \times \exp\{-iS[\boldsymbol{k}-\boldsymbol{A}(t),t',t]\} \tag{8}$$

where $\boldsymbol{A}(t) = (A(t),0,0)$, and $S(\boldsymbol{k},t',t) = \int_{t'}^{t} dt''\{[\boldsymbol{k}+\boldsymbol{A}(t'')]^2/2 - E_0\}$ is the semiclassical action. Neglecting continuum–continuum transitions, the time-dependent dipole moment along x, $D_x(t) = -\langle\Psi(t)|x_1+x_2|\Psi(t)\rangle$ is

$$D_x(t) = -2\int \frac{d^3k dR}{(2\pi)^3}\, d^*_{\rm rec}(\boldsymbol{k},R)\,\chi_0(R)\,\phi(\boldsymbol{k},R,t) + \text{c.c.}, \tag{9}$$

where $d_{\rm rec}(\boldsymbol{k},R) = \langle\exp(i\boldsymbol{k}\cdot\boldsymbol{r}_1)\psi^+(\boldsymbol{r}_2)|x_1|\psi_R(\boldsymbol{r}_1,\boldsymbol{r}_2)\rangle$ is the matrix element for the recombination of the active electron. We note that because we calculate the dipole moment, we have $d_{\rm rec}(\boldsymbol{k},R) = d_{\rm ion}(\boldsymbol{k},R)$.

If one chose to calculate HHG via the momentum or acceleration expectation value instead of the dipole moment, $d_{\rm rec}(\boldsymbol{k},R)$ would have a different form. Actually, the dipole moment as given in equation (9) is not translationally invariant. This is due to using plane wave Volkov solutions, which are not eigenstates of the molecular Hamiltonian and therefore are not orthogonal to the molecular ground state. This lack of orthogonality may induce spurious features in the calculated HG spectrum, e.g. poor description of the interference pattern. A harmonic spectrum calculated from the momentum or acceleration expectation value should reproduce the interference pattern more accurately [29]. The lack of translational invariance is a general undesired feature of the SFA, which becomes more serious in the case of molecules. One way to circumvent the problem is to use formulations which involve less or no position operators (such as acceleration formulation). However, in this work we are mainly concerned with qualitative effects of the vibrational motion on the harmonic spectrum. We note that the structure of our theory does not depend on the use of the dipole moment. A similar structure would emerge within in the acceleration formulation. The use of plane waves in the matrix elements is a wide-spread approximation that becomes more accurate for larger electron wave vectors, which are associated with higher harmonic orders. Naturally, this approach cannot provide a good description of the lowest harmonics.

Using equation (8) in equation (9) one obtains the dipole moment along the

polarization direction,

$$D_x(t) = 2i \int_0^t dt' \int \frac{d^3p}{(2\pi)^3} E(t') \bar{d}[\boldsymbol{p} + \boldsymbol{A}(t)] \bar{d}[\boldsymbol{p} + \boldsymbol{A}(t')] \times C(\boldsymbol{p}, t', t) \exp[-iS(\boldsymbol{p}, t', t)] + \text{c.c.}, \tag{10}$$

where

$$C(\boldsymbol{p}, t', t) = \int dR \, [\eta_{\boldsymbol{p}+\boldsymbol{A}(t)}(R, 0)]^* \eta_{\boldsymbol{p}+\boldsymbol{A}(t')}(R, t - t') \tag{11}$$

is a vibrational correlation function. In the last equation, we have introduced a propagated wave packet $\eta_{\boldsymbol{p}}(R, \tau) \equiv \exp\{-i\hat{H}_R\tau\}\eta_{\boldsymbol{p}}(R)$, to which we will refer as the 'evolved' wave packet below.

Together with equation (11), the dipole moment (10) can be readily understood in terms of a three–step process leading to the emission of harmonics. (a) At time t' the active electron is born in the continuum, while in the remaining molecular ion a vibrational wave packet $\eta_{\boldsymbol{p}+\boldsymbol{A}(t')}(R)$ is launched. The ionization step is described for the active electron by the matrix element $d_{\text{ion}}[\boldsymbol{p} + \boldsymbol{A}(t'), R]$. (b) The detached electron moves in the continuum under the influence of the field only, up to the time t, while acquiring a phase along its trajectory. During the electron motion in the continuum, the vibrational wave packet created in the molecular ion evolves in the corresponding BO potential. (c) At time t, the electron recombines with the molecular ion with the amplitude given by $d_{\text{rec}}[\boldsymbol{p} + \boldsymbol{A}(t), R]$.

In fact, equation (11) is reminiscent of equation (22) of Ref. [30] where the effect of nuclear motion on harmonic generation in H_2^+ was derived in an electronic two-level approach. In our case, the continuum states play the role of the upper electronic state in Ref. [30].

In equation (10), the overlap integral $C(\boldsymbol{p}, t', t)$ captures the vibrational dynamics of the molecular ion. The intensity of a harmonic that is dominated by a single value of the travel time $\tau = t - t'$ is proportional to $|C(\boldsymbol{p}, t', t)|^2$, i.e. the efficiency of the harmonic emission will depend on the overlap between the evolved wave packet $\eta_{\boldsymbol{p}+\boldsymbol{A}(t')}(R, t - t')$ and the 'target' wave packet $\eta_{\boldsymbol{p}+\boldsymbol{A}(t)}(R, 0)$ characterizing the recombination step. [Neglecting the dependence of these vibrational wave packets on the electron momentum, the initial and the target wave packets become identical. In this case, the correlation function, equation (11), becomes an autocorrelation function and the simpler theory of Ref. [20] is recovered.]

The dipole moment (10) can be further simplified by using the saddle point method for the integration over the electron momentum $\boldsymbol{p}$. Assum-

ing that the oscillatory behaviour of the integrand comes only from the exponential of the action, the saddle momentum $\boldsymbol{p}_{\rm s}(t',t)$ is given by the condition $\nabla_{\boldsymbol{p}} S(\boldsymbol{p},t',t)|_{\boldsymbol{p}=\boldsymbol{p}_{\rm s}} = 0$. The saddle momentum reads $\boldsymbol{p}_{\rm s}(t',t) = -\int_{t'}^{t} \boldsymbol{A}(t'')dt''/(t-t')$ and it is such that the position of the electron when it recombines, $\boldsymbol{r}(t)$, is the same as the position when it emerges from under the potential barrier formed by the Coulomb potential and the external field, $\boldsymbol{r}(t')$. We obtain for the dipole moment:

$$D_x(t) = 2i \int_0^t \frac{dt'}{(2\pi)^{3/2}} \frac{E(t')}{[\epsilon + i(t-t')]^{3/2}} \bar{d}[\boldsymbol{p}_{\rm s}(t',t) + \boldsymbol{A}(t)]\bar{d}[\boldsymbol{p}_{\rm s}(t',t) + \boldsymbol{A}(t')] \times C[\boldsymbol{p}_{\rm s}(t',t),t',t] \exp\{-iS[\boldsymbol{p}_{\rm s}(t',t),t',t]\} + \text{c.c.}, \quad (12)$$

with a small cut-off parameter ϵ. The term proportional to $(t-t')^{-3/2}$ is related to the spreading of the electron wave packet.

Both the normalized wave packets and the correlation function can be evaluated numerically assuming the LCAO (linear combination of atomic orbitals) approximation for the electronic ground state of the molecule and of the molecular ion. For the molecular ion, the ground state is taken to be a sum of hydrogenic ground-state wave functions, centred at the positions of the nuclei, with an appropriate normalization factor. For the hydrogen molecule, the ground state is taken to be a product of the molecular-ion ground states, written for each electron. We can then calculate

$$d_{\rm ion}(\boldsymbol{p},R) = i\left[\frac{2}{1+s(R)}\right]^{1/2}\left[-\frac{R_x}{2}\sin\left(\frac{\boldsymbol{p}\cdot\boldsymbol{R}}{2}\right)\tilde{\varphi}(\boldsymbol{p}) + \cos\left(\frac{\boldsymbol{p}\cdot\boldsymbol{R}}{2}\right)\frac{\partial}{\partial p_x}\tilde{\varphi}(\boldsymbol{p})\right], \quad (13)$$

where $\tilde{\varphi}(\boldsymbol{p})$ is the Fourier transform of the hydrogen ground-state wave function and $s(R) = \exp(-R)(3+3R+R^2)/3$ is the overlap integral between two hydrogenic wave functions with centres separated by $\boldsymbol{R}$.

To arrive at a simple picture, we adopt the simple man's model [5] to relate the ionization time t', the recombination time t and the saddle momentum $\boldsymbol{p}_{\rm s}$ to the travel time τ.

Before analyzing separately the cases when the molecular axis is aligned or perpendicular to the field, we describe a few properties of the matrix element (13). We notice that $\lim_{p\to 0} d_{\rm ion}(\boldsymbol{p},R) = 0$. Nevertheless, the limit of the normalized wave packet, $\eta_0(R) = \lim_{p\to 0}\eta_{\boldsymbol{p}}(R)$, exists and can be calculated. It is found to be almost identical to the ground-state vibrational wave function $\chi_0(R)$, see below. The limit of low momenta occurs in the description of the ionization step, when the simple man's model predicts that the initial kinetic momentum of the ionized electron is zero.

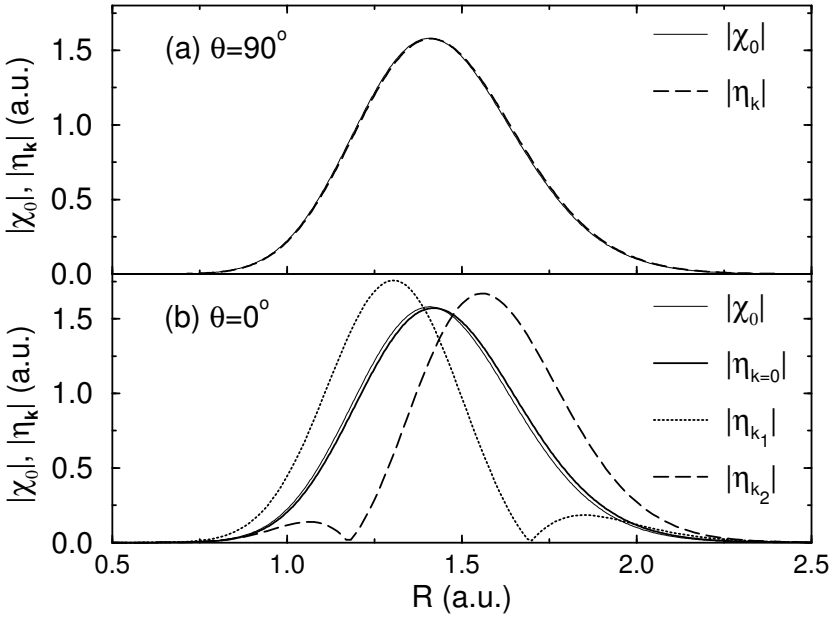

Figure 4. Comparison of the H_2 vibrational ground state $\chi_0(R)$ and the normalized wave packets $\eta_{\boldsymbol{k}}(R)$ for different electron momenta $\boldsymbol{k}$ parallel to the laser field. (a) The molecular axis is perpendicular to the field. The wave packets are independent of the electron momentum and practically identical to the vibrational ground state. (b) The molecular axis is parallel to the field. The electron momenta are such that $k_1^2/2 = 1.6\,U_\mathrm{p}$ and $k_2^2/2 = 3.17\,U_\mathrm{p}$ for laser parameters as in figure 1.

The result of the analysis is shown in figures 4 and 5. When the molecular axis is perpendicular to the field, equation (13) factorizes into functions of the momentum and the internuclear distance. As a consequence, the normalized wave packet will not depend on the electron momentum and, as shown in the upper part of figure 4, it is almost identical to the ground-state vibrational wave function. [The small difference comes from the overlap term $s(R)$ in the normalization factor.] This property, characteristic for the perpendicular case only, is related to the fact that the two-centre interference is always constructive for $\theta = 90°$ [10]. The correlation function (11) then becomes an autocorrelation function (see figure 5 for $\theta = 90°$). At this point, we briefly discuss the electron 'travel time' τ used in figure 5. As we know from the simple man's model, not only one but a few trajectories of the electron, i.e. pairs of ionization time and recombination time, contribute to the emission of a given harmonic.

Between the emission time and the recombination time, the electron acquires kinetic energy under the influence of the field. From all the trajectories that contribute to the emission of a certain harmonic, we choose the one with the shortest duration because for longer travel times the spreading of the electron

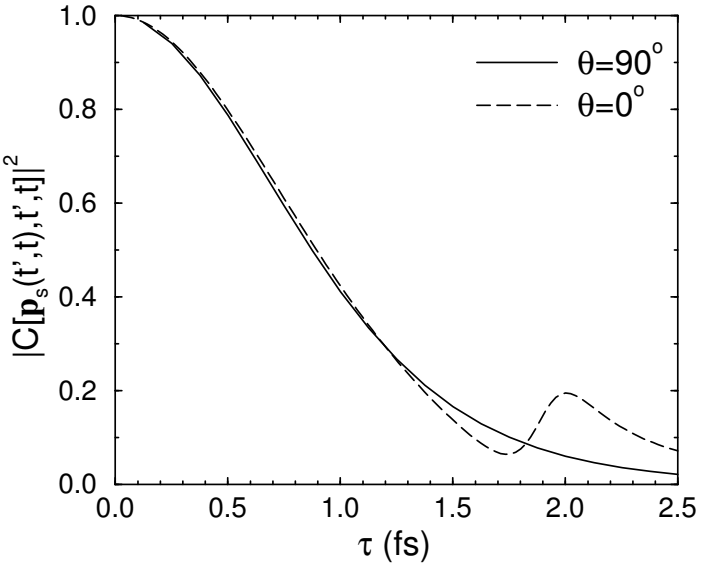

Figure 5. The vibrational correlation function as a function of the electron travel time for two different orientations of the molecular axis. The laser parameters are chosen as in figure 1.

wave packet increases. The shortest travel time for each harmonic increases with increasing harmonic photon energy. Thus, in figure 5, the plotted range of the travel time corresponds to the entire harmonic spectrum covering photon energies from zero to the cut-off energy, $3.17U_\mathrm{p} + I_\mathrm{p}$ [5, 6].

When the molecular axis is aligned with the field, the situation becomes more complicated as compared to perpendicular orientation since now the dipole moment depends on the electron momentum and the internuclear distance in such a way that it cannot be factorized into terms depending separately on both variables. This is related to two-centre interference effects that are sensitive to the projection of the internuclear distance on the field axis. The signature of interference can be observed in panel (b) of figure 4, where the vibrational ground state is shown together with the normalized target wave packets for different energies. We note also that in the limit of low energy, the normalized wave packet is almost identical to the ground state. The two-centre interference leads to a modified behaviour of the correlation function, see figure 5: it exhibits a local minimum and maximum in contrast to the monotonous decay at perpendicular orientation.

The decay of the vibrational correlation function is responsible for the difference between harmonic generation in H_2 and D_2. The nuclear motion is faster in H_2, leading to a more rapid decay of $|C(\boldsymbol{p}, t', t)|^2$ and thus to weaker harmonic emission.

A detailed evaluation of the strong-field approximation for vibrating

molecules will be carried out in future work.

4 Conclusions

By including the nuclear motion in our theoretical description, we take into account the evolution of the molecular core between ionization and recombination of the molecular system. This can have a strong influence on the spectrum of emitted harmonics since the harmonics are sensitive to a vibrational correlation function quantifying the overlap between the evolved nuclear wave packet and a target wave packet that depends on the momentum of the returning electron. In general, this overlap decays quickly with time so that the nuclear motion suppresses the contribution of long electron travel times. The suppression effect is expected to be particularly pronounced in cases such as the H_2^+ molecular ion, where after ionization, the nuclei move in a purely dissociative potential. In the case of molecules such as H_2, where ionization initiates genuine vibrational motion, the situation can be different. Here, one may achieve for certain laser parameters the situation that a window of long travel times is enhanced due to the first return of the vibrational wave packet. These mechanisms provide interesting new perspectives for controlling high-harmonic generation by selection of electron trajectories.

References

[1] H Niikura, F. Légaré, R. Hasbani, A. D. Bandrauk, M. Yu. Ivanov, D. M. Villeneuve and P. B. Corkum, *Nature* **417** 917 (2002).
[2] H. Niikura, F. Légaré, R. Hasbani, M. Yu. Ivanov, D. M. Villeneuve and P. B. Corkum, *Nature* **421** 826 (2003).
[3] A. S. Alnaser, T. Osipov, E. P. Benis, A. Wech, B. Shan, C. L. Cocke, X. M. Tong and C. D. Lin, *Phys. Rev. Lett.* **91** 163002 (2003).
[4] J. Itatani, J. Levesque, D. Zeidler, H. Niikura, H. Pépin, J. C. Kieffer, P. B. Corkum and D. M. Villeneuve, *Nature* **432** 867 (2004).
[5] P. B. Corkum, *Phys. Rev. Lett.* **71** 1994 (1993).
[6] K. C. Kulander, J. Cooper and K. J. Schafer, *Phys. Rev.* A **51** 561 (1995).
[7] T. Zuo, A. D. Bandrauk and P. B. Corkum, *Chem. Phys. Lett.* **259** 313 (1996).
[8] R. Velotta, N. Hay, M. B. Mason, M. Castillejo and J. P. Marangos, *Phys. Rev. Lett.* **87** 183901 (2001).
[9] M. Lein, N. Hay, R. Velotta, J. P. Marangos and P. L. Knight, *Phys. Rev. Lett.* **88** 183903 (2002).
[10] M. Lein, N. Hay, R. Velotta, J. P. Marangos and P. L. Knight, *Phys. Rev.* A **66** 023805 (2002).
[11] M. Lein, P. P. Corso, J. P. Marangos and P. L. Knight, *Phys. Rev.* A **67** 023819 (2003).
[12] G. L. Kamta and A. D. Bandrauk, *Phys. Rev.* A **70** 011404 (2004).
[13] D. Zeidler, J. Levesque, J. Itatani, K. F. Lee, P. W. Dooley, I. V. Litvinyuk, D. M. Villeneuve and P. B. Corkum, in *Ultrafast Optics*, Vol. 4, edited by F. Krausz, G. Korn, P. B. Corkum and I. A. Walmsley (New York: Springer), 259-70 (2003).
[14] R. De Nalda, E. Heesel, M. Lein, N. Hay, R. Velotta, E. Springate, M. Castillejo and J. P. Marangos, *Phys. Rev.* A **69** 031804(R) (2004).
[15] A. Becker, A. D. Bandrauk and S. L. Chin, *Chem. Phys. Lett.* **343** 345 (2001).
[16] X. Urbain et al., *Phys. Rev. Lett.* **92** 163004 (2004).
[17] K. Mishima, K. Nagaya, M. Hayashi and S. H. Lin, *Phys. Rev.* A **70** 063414 (2004).

[18] A. Becker and F. H. M. Faisal, *J. Phys.* B **38** R1 (2005).
[19] T. K. Kjeldsen and L. B. Madsen, *e-print*: physics/0501157 (2005).
[20] M. Lein, *Phys. Rev. Lett.* **94** 053004 (2005).
[21] S. Chelkowski, T. Zuo, O. Atabek and A. D. Bandrauk, *Phys. Rev.* A **52** 2977 (1995); K. C. Kulander, F. H. Mies and K. J. Schafer, *ibid.* **53** 2562 (1996); S. Chelkowski , C. Foisy and A. D. Bandrauk, *ibid.* **57** 1176 (1998); W. Qu, Z. Chen, Z. Xu and C. H. Keitel, *ibid.* **65** 013402 (2001); B. Feuerstein and U. Thumm, *ibid.* **67** 063408 (2003).
[22] M. Lein, T. Kreibich, E. K. U. Gross and V. Engel, *Phys. Rev.* A **65** 033403 (2002).
[23] T. Kreibich, M. Lein, V. Engel and E. K. U. Gross, *Phys. Rev. Lett.* **87** 103901 (2001).
[24] W. Kołos, K. Szalewicz and H. J. Monkhorst, *J. Chem. Phys.* **84** 3278 (1986).
[25] M. D. Feit, J. A. Fleck, Jr. and A. Steiger, *J. Comput. Phys.* **47** 412 (1982).
[26] K. Burnett, V. C. Reed, J. Cooper and P. L. Knight, *Phys. Rev.* A **45** 3347 (1992).
[27] M. Lein et al., *J. Mod. Opt.* **52** 465 (2005).
[28] M. Lewenstein, P. Balcou, M. Y. Ivanov, A. L'Huillier and P. B. Corkum, *Phys. Rev.* A **49** 2117 (1994).
[29] G. Lagmago Kamta and A. D. Bandrauk, *Phys. Rev.* A **71** 053407 (2005).
[30] E. E. Aubanel, T. Zuo and A. D. Bandrauk, *Phys. Rev.* A **49** 3776 (1994).